

# Fundamental studies on a planar-cathode direct current glow discharge. Part II: numerical modeling and comparison with laser scattering experiments<sup>☆</sup>

Annemie Bogaerts<sup>a,\*</sup>, Renaat Gijbels<sup>a</sup>, Gerardo Gamez<sup>b</sup>, Gary M. Hieftje<sup>b</sup>

<sup>a</sup>Department of Chemistry, University of Antwerp, Universiteitsplein 1, B-2610 Antwerp, Belgium

<sup>b</sup>Department of Chemistry, Indiana University, Bloomington, IN 45405, USA

Received 1 October 2003; accepted 3 December 2003

## Abstract

We have calculated the gas temperature, electron density, electron energy distribution function, and average electron energy, as a function of distance from the cathode, with a two-dimensional model for an argon direct-current glow discharge. The calculated results are compared with measured values from Rayleigh- and Thomson-scattering experiments, for different values of voltage, pressure and electrical current. The gas-temperature distribution and electron-density profile were found to be in reasonable agreement with experiment. For the electron energy, model and experiment give complementary information, since the experiment is able to detect only the thermal and low-energy electrons, whereas the model focuses mainly on the high-energy electrons.

© 2003 Elsevier B.V. All rights reserved.

**Keywords:** Glow discharge; Modeling; Gas temperature; Electron density; Electron energy distribution function; Electron energy

## 1. Introduction

Glow discharges have been used for decades in analytical spectrometry, mainly for solid-sample analysis [1–3]. For good analytical practice, a better insight into the plasma behavior is desirable. This can be obtained by experiments (see e.g. in Ref. [4]), and also by numerical modeling. In previous years, we have developed a comprehensive modeling network for analytical glow discharges in argon with a copper cathode, in d.c., r.f. and (millisecond and microsecond) pulsed modes (see, e.g. in Refs. [5,6] and references therein). Typical results of the calculations include the electrical characteristics (voltage–current–pressure relations, also as a function of time, in the case of r.f. or pulsed mode), the

gas temperature, the electric field and potential distribution in the plasma, the densities, fluxes and energies of the various plasma species, information about the collision processes in the plasma, and about the production and loss mechanisms of the various species, erosion rates and crater profiles due to sputtering at the cathode, optical emission intensities, etc. These calculated results have been compared as much as possible with experimental data, to check the validity of the models. More specifically, comparisons have been made for sputtered atom and ion densities [7,8], argon metastable atom densities [9], electron densities [10], crater profiles [11] and erosion rates [11,12], optical emission intensities [12,13], and current–voltage–pressure relations (e.g. in Ref. [14]); in general, reasonable agreement has been reached between calculated and measured results.

However, there are still uncertainties in the model. For example, the secondary-electron emission coefficient at the cathode is used as an input parameter in the model, but its value is not known very well. Indeed, it can depend greatly on the cathode surface condition (i.e. kind of material, surface roughness, surface contaminants), as well as on the bombarding particle energy

<sup>☆</sup>This paper was presented at the Presymposium on Sample Introduction in Atomic Spectrometry of the Colloquium Spectroscopicum Internationale XXXIII in Spain. The presymposium was held in Zaragoza, 3–6 September 2003. This paper is published in the special issue of *Spectrochimica Acta Part B*, dedicated to the CSI XXXIII.

\*Corresponding author.

E-mail address: [annemie.bogaerts@ua.ac.be](mailto:annemie.bogaerts@ua.ac.be) (A. Bogaerts).

Table 1

Overview of the different plasma species taken into account in the modeling network, and the models used to describe their behavior

Plasma species	Models
Ar gas atoms	Heat conduction equation for gas temperature
Fast (energetic) electrons	Monte Carlo model
Thermal electrons	Fluid model
Ar <sup>+</sup> ions	Fluid model
Fast Ar <sup>+</sup> ions in CDS	Monte Carlo model
Fast Ar atoms in CDS	Monte Carlo model
Ar atoms in 64 excited levels	Collisional-radiative model
Sputtering at cathode	Empirical formula + energy distributions
Thermalization of sputtered Cu atoms	Monte Carlo model
Cu atoms in ground state and 7 excited levels	Collisional-radiative model
Cu <sup>+</sup> ions in ground state and 6 excited levels	Collisional-radiative model
Fast Cu <sup>+</sup> ions in CDS	Monte Carlo model

[15]. However, this parameter can have a large effect on the calculated results. Indeed, a higher secondary-electron emission coefficient yields more electrons created at the cathode as a result of ion (or atom) bombardment. These electrons give rise to more ionization collisions, creating more electron–ion pairs, and the ions result again in more secondary-electron emission upon bombardment at the cathode. Hence, a higher secondary-electron emission coefficient will result in higher densities and fluxes of electrons and ions, and other plasma species, and also in higher electrical currents for the same voltage and pressure [16]. In many glow discharge models (e.g. in Refs. [17–20]), a constant secondary electron emission coefficient is assumed, and sometimes this value is used as a ‘tuning parameter’ to obtain calculated current–voltage–pressure relations in agreement with experimental data.

Another uncertainty in the model is the gas temperature. This value cannot easily be measured in the plasma, but it can also have a strong effect on the calculations. Indeed, a lower gas temperature yields a higher argon gas density  $n$  (from the ideal gas law:  $n = p/kT$ ). This higher density can give rise to more collisions, including more ionization collisions, and hence more creation of electron–ion pairs. These extra electrons give rise to more electron-impact ionization, and the extra ions result in greater secondary electron emission. Hence, a lower gas temperature yields higher densities and fluxes of electrons, ions and other plasma species, and also a higher electrical current, for the same voltage and pressure. The gas temperature can be calculated from the heat conduction equation [21], but in order to do so, the temperature at the cathode surface should be known, and the latter is also subject to uncertainties. Therefore, this shifts the problem of unknown gas temperature to unknown cathode temperature.

These uncertainties in the model illustrate the need to have more and better experimental data, more specifically for the gas temperature, and for the electrical characteristics (current–voltage–pressure relations) at a

given gas temperature. Indeed, when the current–voltage–pressure relations are correctly predicted, the other calculated results, such as the densities of plasma species, which are more difficult to measure, will probably also be in the correct order of magnitude.

In Ref. [4]—heretofore referred to as Paper I—the gas temperature was measured as a function of position from the cathode, for different values of voltage, pressure and current. By comparing these experimental results with our calculations, we can check whether the correct processes and input data (collision cross-sections, secondary electron emission coefficient) are utilized in our model. Moreover, from the comparison of measured and calculated gas temperature, we hope to obtain some information about the cathode temperature. The latter can then also be compared with estimated values from the experiments. Besides the gas temperature, we will also focus in the present paper on the calculated electron density, electron energy distribution function (EEDF) and mean electron energy, because these calculated results can also be compared with the measurements from Paper I.

## 2. Description of the model

The comprehensive modeling network that we have developed in previous years for an Ar glow discharge with Cu cathode, consists of a number of ‘sub-models’ for the various plasma species, as shown in Table 1. More information about these models can be found e.g. in Refs. [5,6] and the references therein. In the present paper, we will focus on only those models that are directly relevant for the plasma quantities that we want to compare with experimental data, i.e. the electrical characteristics, the electron behavior, and the gas temperature.

### 2.1. Monte Carlo model for the fast (i.e. non-thermal) electrons

The electrons are emitted from the cathode by secondary electron emission, and they are accelerated away

from the cathode by the strong electric field in the cathode dark space (CDS). During successive time-steps, the trajectory of the individual electrons is followed with Newton's laws, and the collisions during that time-step (i.e. occurrence of a collision, kind of collision, and new energy and direction after collision) are treated with random numbers. In order to achieve statistically valid results, a large number of electrons have to be followed. The electrons to be followed are called 'super-electrons', and they represent a certain number of real electrons. The collisions taken into account are elastic collisions with Ar gas atoms, electron-impact ionization and excitation of Ar atoms in the ground state and in various excited levels, and of sputtered (Cu) atoms, as well as electron–electron Coulomb scattering. The electrons are followed in this Monte Carlo model until they reach the walls (where they can be absorbed, reflected, or cause secondary electron emission), or until their total energy (i.e. sum of potential and kinetic energy) drops below the threshold for inelastic collisions. In the latter case, the electrons are transferred to the thermal electron group, treated in the fluid model (see below). More information about this Monte Carlo model can be found e.g. in Refs. [20,22].

## 2.2. Fluid model for the thermal electrons and Ar<sup>+</sup> ions

The behavior of the thermal electrons is described with a fluid model, which also treats the Ar<sup>+</sup> ions. The model consists of the continuity equations for electrons and Ar<sup>+</sup> ions, and their flux equations, based on diffusion and on migration in the electric field. These four equations are coupled to Poisson's equation for a self-consistent calculation of the electric-field distribution. More details about this model are given e.g. in Ref. [20].

## 2.3. Monte Carlo model for the fast (energetic) Ar<sup>+</sup> ions and Ar atoms in the CDS

The Ar<sup>+</sup> ions are treated not only with a fluid model, but they are also followed with a Monte Carlo model in the CDS. Moreover, the behavior of the energetic Ar atoms, created from elastic collisions (including charge transfer collisions) of the Ar<sup>+</sup> ions with Ar gas atoms, is also described with a Monte Carlo model. The benefit of these Monte Carlo models is that they can provide information on the energy distributions of the Ar<sup>+</sup> ions and fast Ar atoms bombarding the cathode, which are necessary to calculate the sputtering rate. Moreover, the Ar<sup>+</sup> ions and fast Ar atoms can also give rise to ionization in the CDS, and hence to the formation of new electron–ion pairs. It was demonstrated that the latter ionization mechanisms have a significant effect on

the calculated current–voltage–pressure relations [23]. This model is explained in more detail in Refs. [22,23].

## 2.4. Monte Carlo model for thermalization of the sputtered Cu atoms

As mentioned above, the sputtering rate, or the flux of Cu atoms sputtered from the cathode, is calculated from the energy distributions of the Ar<sup>+</sup> ions, fast Ar atoms, as well as Cu<sup>+</sup> ions bombarding the cathode, multiplied by the sputter yield as a function of bombarding energy, calculated with an empirical formula [24]. When the Cu atoms are sputtered, they have typical energies of 5–10 eV, which they lose rapidly by collisions with the Ar gas atoms, until they are thermalized. This thermalization process is described again with a Monte Carlo model (see Ref. [25] for more information).

## 2.5. Heat conduction equation for the Ar gas heating

The fast Ar<sup>+</sup> ions, Ar atoms and Cu atoms transfer energy to the Ar background gas as a result of elastic collisions (see above; Sections 2.3 and 2.4). This leads to heating of the Ar gas. The Ar gas temperature distribution in the plasma is calculated from a heat-conduction equation, in which the source terms are given by the power input, calculated in the above Monte Carlo models, i.e. from the elastic collisions of the energetic plasma species with the Ar gas atoms, and from thermalization of the energetic Ar atoms, as a result of elastic collisions with the Ar gas atoms. More details about this model, as well as about the coupling with the other models described above, can be found in Ref. [21].

## 3. Results and discussion

The calculations are performed for a glow-discharge geometry similar to that described in Paper I and in Ref. [26], but a few simplifications are made, which probably do not affect the presented results. Indeed, in the model we assume the same cathode and anode diameter (i.e. 1.2 cm and 5 cm, respectively), and the same distance between anode and cathode (i.e. 5 cm) as in the experiment, but instead of a large cell housing at floating potential, we assume a simple cylindrical cell at anode potential, and with diameter equal to the anode diameter.

The calculations are performed for exactly the same conditions as used in the experiment (see Paper I). In the model, the gas pressure and the discharge voltage are used as inputs, whereas the gas temperature and electrical current are calculated. The latter is computed as the sum of the charged particle fluxes. In our calculations, we assume a constant secondary electron

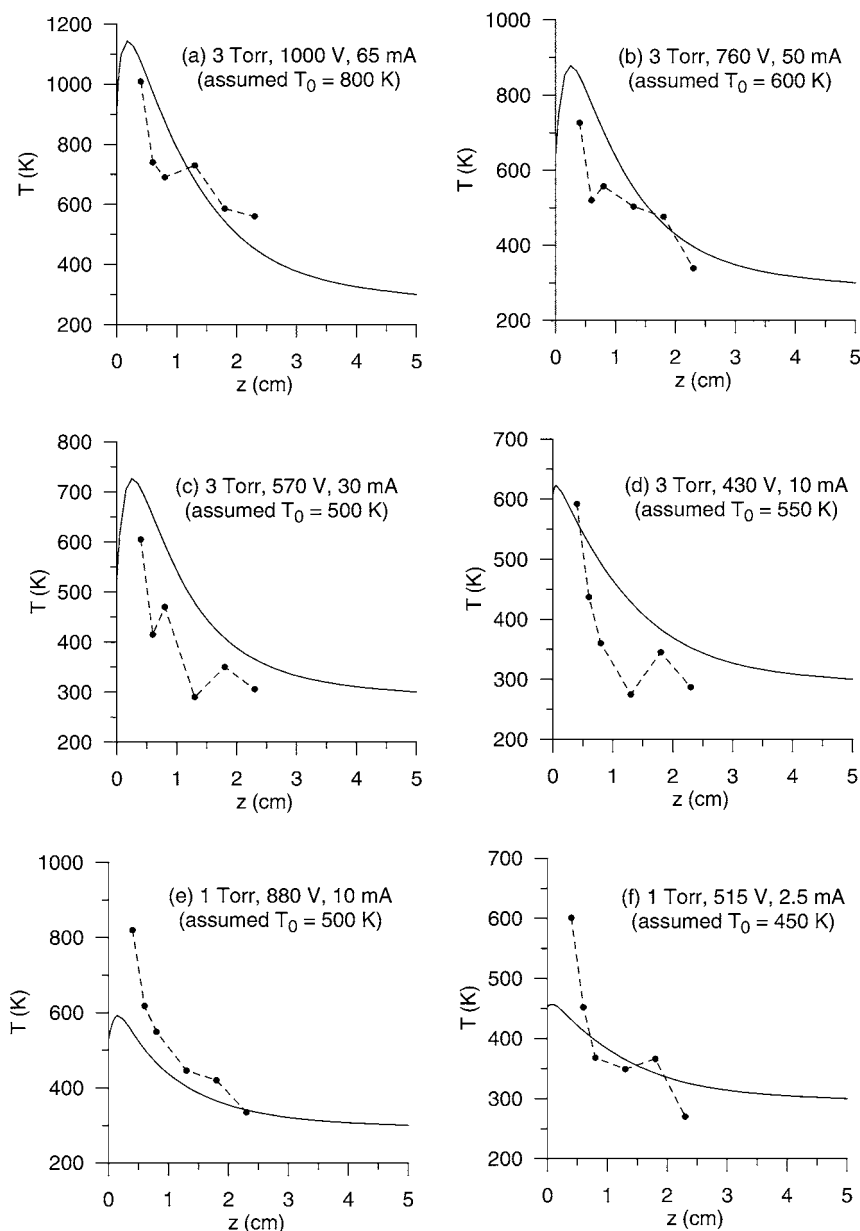


Fig. 1. Calculated (solid lines) and experimental (from Rayleigh scattering; dashed lines + symbols) gas temperature distributions, at six different glow discharge conditions. The assumed values for the cathode temperature ( $T_0$ ) are also indicated in each case.

emission coefficient of 0.07, which is typical for  $\text{Ar}^+$  ion bombardment on clean (i.e. sputter-cleaned) cathode surfaces [15]. Both the calculated gas temperature, and the resulting current as a function of voltage and pressure will be compared with experiment, to check the results of the numerical simulation.

### 3.1. Gas temperature

Fig. 1 shows the calculated gas temperature distributions (solid lines) for the six different experimental operating conditions, in comparison with the data obtained from the Rayleigh scattering experiments of

Paper I (dashed lines + symbols). In general, the agreement is reasonable. It appears that at 3 Torr, the calculated results are somewhat higher than the experimental data, whereas at 1 Torr, the opposite is found. Both experimental and calculated values are close to 300 K far away from the cathode, but they reach high values near the cathode. At low current and voltage (e.g. 515 V and 2.5 mA at 1 Torr), the calculated and experimental temperatures are in the order of 400–500 K, a value that increases to approximately 1000 K at high voltage and current (e.g. 1000 V and 65 mA at 3 Torr). These values are somewhat lower but still in reasonable correspondence with gas temperature data

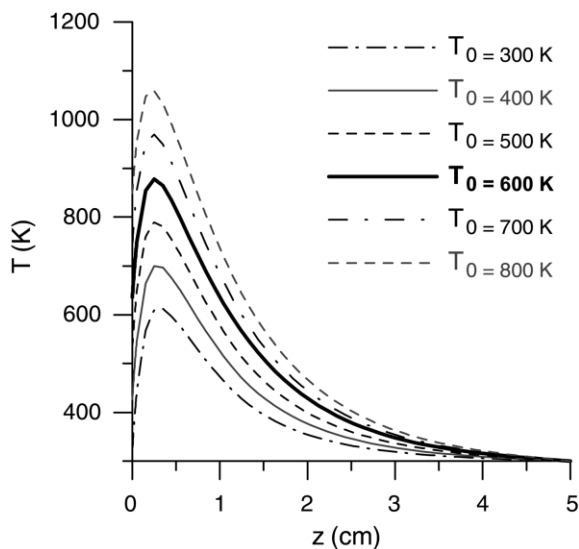


Fig. 2. Calculated gas temperature distributions, at 3 Torr, 760 V and 50 mA, for different input values of the cathode temperature ( $T_0$ ). The thick solid line (with  $T_0=600$  K) was presented in Fig. 1b.

reported in the literature for Grimm-type glow discharges, measured from the Doppler width of optical emission intensities [27,28].

It is important to mention that the calculated gas temperature depends strongly on the assumed cathode temperature (see also Ref. [21]). Therefore, the cathode temperature values ( $T_0$ ) assumed for our gas temperature calculations are also indicated in Fig. 1.

The effect of the cathode temperature on the calculated gas temperature is also illustrated for 3 Torr, 760 V and 50 mA in Fig. 2. A higher cathode temperature ( $T_0$ ) results in a higher gas temperature, and the effect is almost linear. Indeed, when  $T_0$  increases by 100 K, the maximum gas temperature rises by approximately 90 K. Hence, at  $T_0=300$  K, the maximum gas temperature is approximately 610 K, and at  $T_0=800$  K, the maximum gas temperature is 1060 K. This shows that the calculated gas temperature is very sensitive to the input value of the cathode temperature, which illustrates the weakness of the model, since the cathode temperature is generally not known (although in Paper I, an experiment was performed to measure the cathode temperature under one set of conditions [4]). Therefore, we have used the cathode temperature as a kind of adjustable parameter to obtain a gas temperature distribution, which yields satisfactory agreement between calculated and measured electrical currents. For the conditions of Fig. 2, this is the case for the gas temperature represented by the thick solid line (with  $T_0=600$  K). Since this gas temperature is in satisfactory agreement with the experimental data (see Fig. 1b), this suggests that the model can give reasonable predictions for the electrical current as a function of voltage, pressure and gas temperature,

and hence that other calculated results, such as plasma species densities and fluxes, will also be rather well predicted (see Section 1).

Furthermore, all  $T_0$  values indicated in Fig. 1 are realistic (although at 3 Torr and 65 mA, a somewhat lower cathode temperature (between 545 and 600 K) was obtained from the experiment – see Paper I [4]). Moreover, in general the  $T_0$  values increase with rising electrical current, as is expected. Hence, this shows that the cathode temperature assumed in our model is in fact more than simply an adjustable parameter, but that it also has a realistic physical meaning.

Finally, the reasonable agreement between the calculated and measured gas temperature for the assumed values of the cathode temperature indicated in Fig. 1 suggests that the cathode surface temperature can be quite high, even when water cooling is applied. This would suggest that the cooling in the experiment of Paper I is perhaps not very efficient. Indeed, in this experiment, the cooling is applied only from the backside of the sample, and possibly the contact between the sample and cooling block is not perfect.

Since our modeling network is in fact two-dimensional (for a cylindrically symmetrical symmetry) it provides information not only on the axial dependence of the plasma quantities, but also on the radial variation. In Fig. 3, the two-dimensional temperature distribution is plotted, for 3 Torr, 760 V and 50 mA. The black rectangle at  $z=0$  cm and approximately  $r=0$  cm symbolizes the cathode, whereas the other borders of the

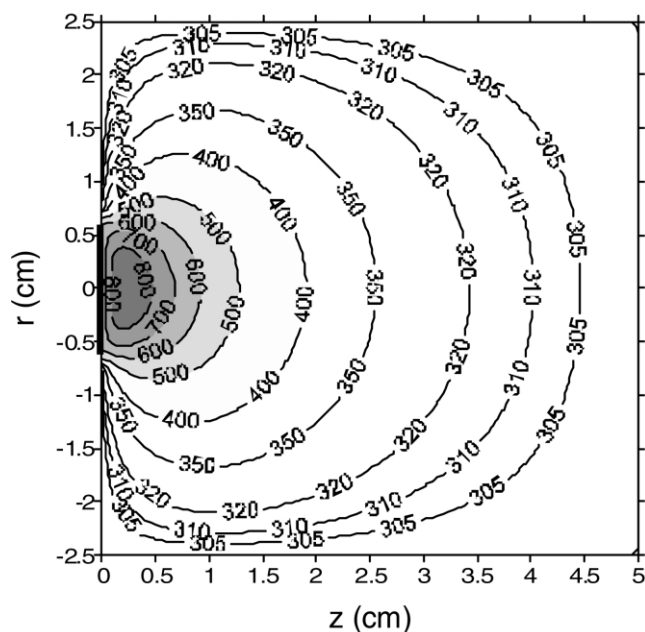


Fig. 3. Calculated two-dimensional gas temperature distribution, at 3 Torr, 760 V and 50 mA. The cathode is symbolized with the black rectangle at  $z=0$  cm and approximately  $r=0$  cm, whereas the other borders of the figure represent the anode walls.

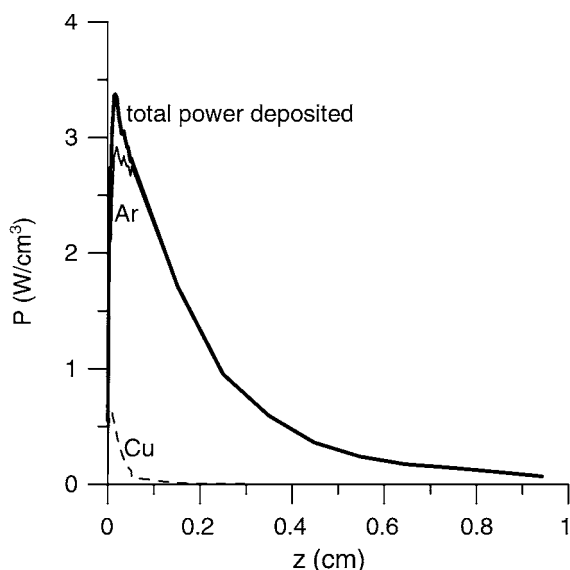


Fig. 4. Calculated power deposited in the Ar gas, used for gas heating, as a function of position from the cathode, at 3 Torr, 760 V and 50 mA. Also shown are the contributions by thermalization of energetic Ar atoms (solid line), and by direct energy input into the Ar gas, due to elastic collisions of sputtered Cu atoms with Ar gas atoms (dashed line).

figure represent the anode walls. It is clear that the gas temperature varies not only in the axial direction, but also drops significantly in the radial direction, to a value of 300 K near the anode walls. Indeed, 300 K was assumed as the anode wall temperature in our model. Hence, the highest gas temperature is observed on the cell axis, and especially in the region defined by the cathode diameter.

As mentioned in Section 2, the gas heating is the consequence of elastic collisions of energetic  $\text{Ar}^+$  ions, Ar atoms and Cu atoms with Ar gas atoms. Fig. 4 illustrates the total power deposited in the Ar gas as a function of position from the cathode. It is clear that most energy input into the Ar gas takes place near the cathode, where the energetic plasma species have their highest energy. This explains the peak in the calculated gas-temperature profile near the cathode (see Figs. 1–3). The energy input into the Ar gas becomes negligible beyond approximately 1 cm from the cathode. From Fig. 4, it follows also that most of the power deposition comes from energetic Ar atoms (thin solid line), more specifically from their thermalization as a result of elastic collisions with the Ar gas atoms. Indeed, in the Monte Carlo models for fast  $\text{Ar}^+$  ions, fast Ar atoms and Cu atoms, elastic collisions with Ar gas atoms can give rise either to the creation of fast Ar atoms, or directly to gas heating, defined by a certain threshold (see Ref. [21] for more explanation). For the threshold value assumed in our model (i.e. three times the thermal energy), it was found that direct energy input into the

Ar gas due to elastic collisions is of minor importance, but that mainly fast Ar atoms are created in these collisions, which subsequently will thermalize as a result of further elastic collisions. The latter thermalization was found to be the most important for determining the gas heating. It is clear that when this threshold value is increased, the relative contribution of direct energy input by elastic collisions will rise as well, compared to the energy input due to thermalization. However, the resulting gas-temperature profile was found to be very similar, for different assumptions of this threshold value, as is seen in Fig. 5 (for the same operating conditions as under study here). It should be mentioned, however, that the only direct energy transfer into the Ar gas that plays a role for the gas heating, beside the thermalization of the fast Ar atoms, is given by elastic collisions of the sputtered Cu atoms with the Ar gas atoms, which occurs very close to the cathode, as is illustrated in Fig. 4 (dashed line). Finally, it is interesting to note that energy transfer from elastic collisions of energetic electrons with the Ar gas is found to contribute negligibly to gas heating, due to the large difference in mass between electrons and Ar gas atoms [21].

For the conditions under study (i.e. 3 Torr, 760 V and 50 mA), the total power deposited into the Ar gas, and used for gas heating, is approximately 1.5 W, when integrated over the entire discharge cell, whereas the

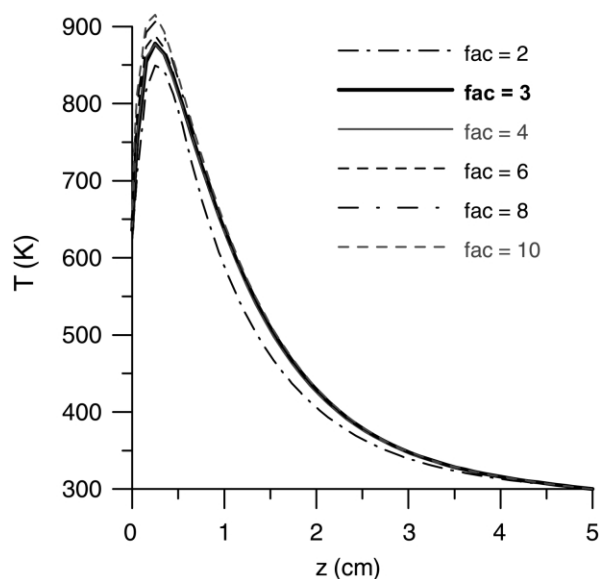


Fig. 5. Calculated gas temperature distributions, at 3 Torr, 760 V and 50 mA, for different values of the threshold energy assumed for either direct power deposition into the Ar gas, or formation of energetic Ar atoms (e.g.  $\text{fac}=2$  means that when the energy of an Ar atom after an elastic collision is higher than two times the thermal energy, a fast Ar atom is created, and when the energy of the Ar atoms is lower than two times the thermal energy, the energy is deposited into the Ar gas, used for gas heating). The thick solid line (with  $\text{fac}=3$ ) was presented in Fig. 1b.

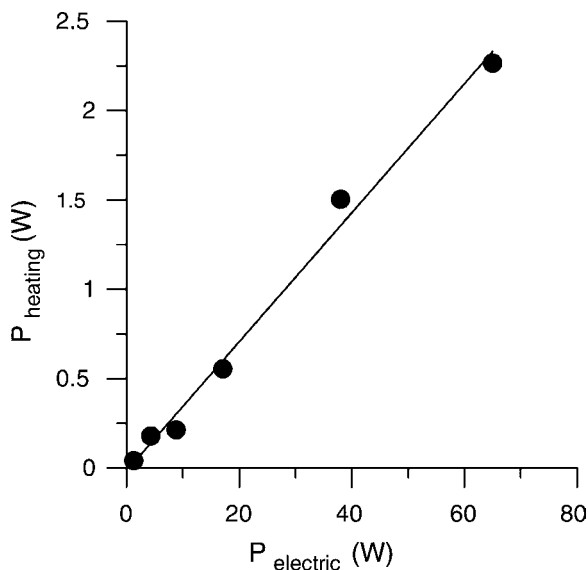


Fig. 6. Calculated total power deposited into the Ar gas, used for gas heating, as a function of the electrical power in the glow discharge, for the six different glow discharge conditions.

electrical power is 38 W. Hence, it appears that approximately 4% of the electrical power is used for heating of the Ar gas. This fraction seems to be typical for all conditions investigated. Indeed, in Fig. 6, the power used for heating is plotted against the electrical power, and a more or less linear relationship is found, with the power used for heating typically approximately 2.5–4% of the electrical power. Similar results were obtained also in Ref. [21], for glow discharge conditions characteristic for the VG9000 glow discharge mass spectrometer, and for a Grimm-type glow discharge cell.

### 3.2. Electron density and energy

Fig. 7 shows the calculated electron density profiles for the six different conditions under study. The electron density was also measured in the Thomson-scattering experiment (see Paper I), at 3 Torr, 1000 V and 55 mA, at 3 Torr, 520 V and 35 mA, and at 1 Torr, 600 V and 5 mA, and these results are also presented in Fig. 7a, c and f, respectively.

In the Rayleigh-scattering experiment (i.e. for the gas temperature measurements), a voltage of 1000 V at 3 Torr yielded a somewhat higher current of 65 mA (see above; Fig. 1a). The reason for the lower current in the Thomson-scattering experiment is that the latter took a much longer time, and a small drift in the current towards lower values was observed as a function of time. Moreover, to obtain the whole Thomson-scattering profile, the cathode had to be replaced a couple of times and, as discussed in the Section 1, the secondary electron emission coefficient, which determines the electrical current as a function of voltage and pressure, depends

on the surface conditions of the cathode material. Finally, the Rayleigh- and Thomson-scattering experiments had to be carried out on different days, because of the long time required to record the Thomson-scattering spectrum, and there is a certain day-to-day variability in the electrical conditions. Since we have performed our calculations for the conditions of the Rayleigh-scattering experiments, the calculated and experimental electron densities pertain to somewhat different conditions (as indicated in Fig. 7a, c and f), but a comparison can still be made.

The calculated electron density is very low near the cathode, in the CDS, because the electrons are accelerated here by the strong electric field. The density reaches a pronounced maximum at the beginning of the negative glow (NG), i.e. at approximately 1 mm from the cathode, and then drops significantly as a function of distance from the cathode, to very low values approximately 2 cm from the cathode. The experimental result at 3 Torr, 35 mA and 520 V is also characterized by a similar profile (see Fig. 7c), but the results at 3 Torr, 55 mA and 1000 V, do not show this pronounced peak. This might illustrate that the Thomson-scattering experiments are subject to some uncertainties, because the electron densities in glow discharges are rather low, and the measurements are not at all straightforward (e.g. a number of precautions have to be made to have a strong-enough Thomson-scattering signal, as discussed in Paper I and in Ref. [26]).

The calculated electron density at 3 Torr, 1000 V and 65 mA (Fig. 7a) is higher than the experimental result, but the current is also slightly higher, so the disparity should be corrected for this difference. The correlation between calculations and experiment at 1 Torr (Fig. 7f) is reasonable, and at 3 Torr, 570/520 V and 30/35 mA (Fig. 7c) a very good agreement is found.

As Fig. 7 shows, the calculated electron density increases with rising voltage and current, as well as with rising pressure, as expected. The calculated values range from  $4 \times 10^{11} \text{ cm}^{-3}$  at the lowest voltage, pressure and current investigated (i.e. 1 Torr, 515 V, 2.5 mA), to approximately  $10^{13} \text{ cm}^{-3}$  at the highest voltage, pressure and current under study (i.e. 3 torr, 1000 V, 65 mA).

In the literature, measurements of electron densities in glow discharges have also been reported by Stark spectroscopy [27–29] and by Langmuir-probe experiments [30–32]. The Stark-spectroscopy experiments yielded electron densities on the order of  $10^{14} \text{ cm}^{-3}$ , i.e. higher than our present calculated and measured values, but the pressure was also somewhat higher. However, Marcus et al. reported electron densities varying from  $6 \times 10^{10}$  to  $2 \times 10^{11} \text{ cm}^{-3}$ , obtained from Langmuir-probe measurements, for conditions of 2–3 Torr, 500–700 V, and 5–15 mA [30,31]. These values are somewhat lower than ours. However, the electron density depends not only on pressure, voltage and

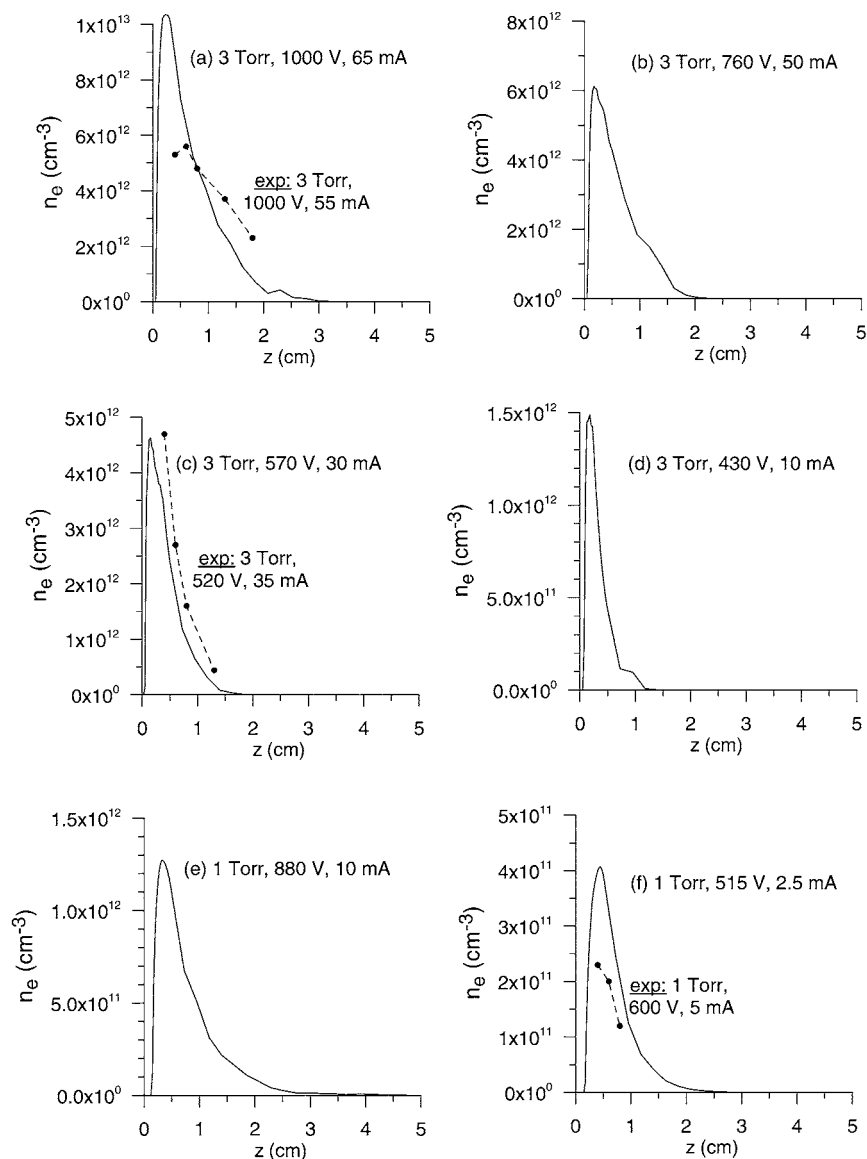


Fig. 7. Calculated electron density profiles (solid lines), at six different glow discharge conditions. In figure (a), (c) and (f), comparison is made with the measured values from Thomson scattering experiments (dashed lines + symbols).

current, but also strongly on the cathode size (which determines the current density), and it varies also with distance from the cathode (see Fig. 7). Hence, comparison with literature data makes sense only when all parameters (including the position of measurement in the plasma) are the same. With our modeling network, we have calculated electron densities varying from 10<sup>11</sup> to 10<sup>14</sup> cm<sup>-3</sup>, for glow-discharge conditions in the range of 500–1400 V, 0.4–5 Torr, and 1–100 mA (see e.g. in Refs. [33,34]). For typical Grimm-type glow-discharge conditions (i.e. 500–1200 V, 2–5 Torr and 10–100 mA), our calculated electron densities were found to be in good agreement with data obtained from Langmuir-probe measurements [32,33]. The latter observation, in combination with the present reasonable agree-

ment with the Thomson scattering measurements, illustrates that the electron densities obtained with our model can be considered as realistic.

The Thomson-scattering experiment provides information not only on the electron density, but also on the electron energy distribution function (EEDF). Two electron groups could be distinguished, i.e. a thermal energy group (approx. 0.3 eV) and an energetic electron group (with energy approx. 1 eV) [4]. In our model, we also calculate the EEDF, but the latter ranges from thermal energy to the maximum energy, corresponding to the discharge voltage. In fact, the calculated EEDF in our model is more reliable at higher energies than at thermal energy, because it is obtained with the Monte Carlo model, which is most suitable for non-thermal electrons.

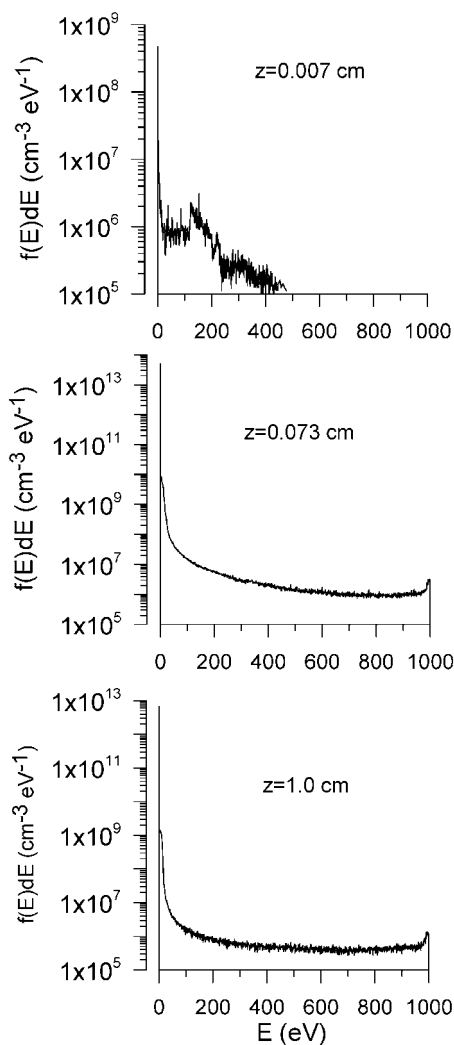


Fig. 8. Calculated electron energy distribution functions, at three different distances from the cathode, at 3 Torr, 1000 V and 65 mA ( $z=0.073$  cm indicates the CDS/NG interface).

Of course, the electrons with energy above the threshold for inelastic collisions (e.g. 15.76 eV for ionization of ground-state Ar atoms, 11.55 eV for excitation of ground-state Ar atoms to the lowest excited levels, 4.21 eV for ionization of the Ar metastable levels,...) are particularly important for the glow discharge. Indeed, they give rise to excitation (i.e. creation of excited levels, which is relevant for optical emission spectrometry) and to ionization (i.e. creation of electron–ion pairs), and are therefore important for sustaining the discharge. These energetic electrons were, however, not observed in the experiments, because their fraction is quite low compared to the thermal electrons (see below), and the sensitivity of the experiments is not sufficient to observe them.

The calculated EEDF, at three different distances from the cathode, is plotted in Fig. 8 for the conditions of Fig. 7a (i.e. 3 Torr, 1000 V and 65 mA). Note that the

Y-axis is slightly shifted to the left, so that the behavior at thermal energy can be clearly distinguished. It follows from this figure that the EEDF is at maximum at thermal energy; it drops quickly at rising energy up to approximately 20 eV, and then more slowly for higher energies. At  $z=0.007$  cm, i.e. close to the cathode, the absolute value of the EEDF and the statistics are not so good, because there are not many electrons present here, as they are rapidly accelerated away from the cathode by the strong electric field. Also, the maximum energy is limited, because the electrons have not yet traversed the entire CDS, and could not yet have gained the maximum possible energy from the potential drop. At the end of the CDS, i.e. at  $z=0.073$  cm, the EEDF ranges from thermal energy to 1000 eV, i.e. corresponding to the discharge voltage. Indeed, the electrons can have gained the total energy from the potential drop, at least if they have traversed the entire CDS without any collisions. However, most of the electrons have lower energy, because they have lost energy in several collisions. Statistics are now much better, and the absolute value of the EEDF is higher, because the electron density is quite high at the end of the CDS – beginning of NG. At  $z=1$  cm, i.e. somewhere in the NG, the EEDF looks very similar to the profile at the end of the CDS, but the absolute value is slightly lower, because the density is lower (see Fig. 7a and below). Moreover, the EEDF drops more rapidly towards higher energy, because the electrons have already lost additional energy by collisions in the NG. Although, neither the Thomson-scattering experiments nor the Langmuir-probe measurements are able to record the entire EEDF up to the maximum energy corresponding to the discharge voltage, due to limited sensitivity, such measurements have been reported with a differentially pumped retarding-field analyzer, in a He glow discharge [35]. The EEDF measured in this experiment was also found to range from thermal to the maximum energy corresponding to the discharge voltage, and a small peak at maximum energy was even observed at the CDS/NG boundary [35]. Hence, although for a different gas and somewhat different conditions, this experimental result can be seen as a qualitative validation for our calculated EEDFs.

The electron density profiles shown in Fig. 7 were obtained from the fluid model, which deals with the thermal electrons. The Monte Carlo model can, however, also provide information on the electron density. In principle, the density obtained with the Monte Carlo model should reflect the total electron density, but because the latter model is not ideal for thermal electrons (because it would require too long a computation time), it yields only the non-thermal electron density. This is illustrated in Fig. 9 for the same conditions as in Fig. 8 (i.e. 3 Torr, 1000 V, 65 mA). The non-thermal electron density is characterized by a similar profile as the thermal electron density, i.e. with low values in the

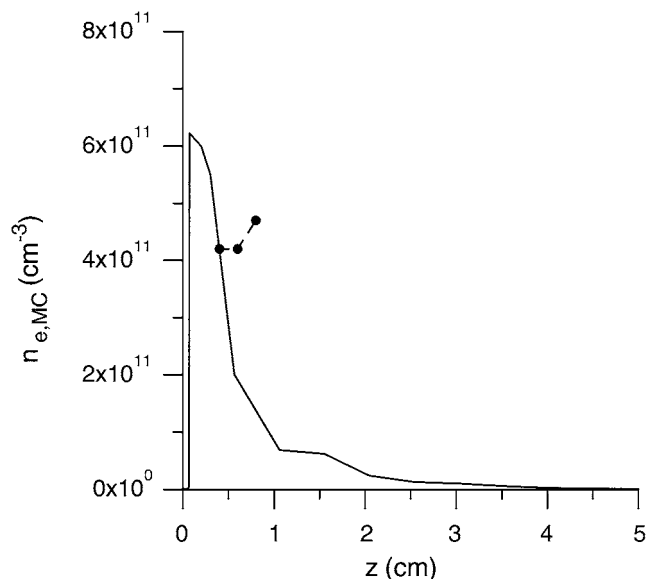


Fig. 9. Calculated electron density profile, obtained from the Monte Carlo model, and representing the non-thermal electrons, at 3 Torr, 1000 V and 65 mA (solid line), and comparison with the measured non-thermal electron density from Thomson scattering experiments (dashed lines + symbols), at 3 Torr, 1000 V and 55 mA.

CDS, and a maximum in the beginning of the NG. Furthermore, the non-thermal electron density is clearly lower than the thermal electron density presented in Fig. 7a, which is as expected, and which is in correlation with the experimental observations. Indeed, Fig. 9 also shows the measured non-thermal electron density. From the three experimental points, it is not straightforward to deduce a density profile. The latter seems to be different from the calculated electron density profile, but the absolute values of calculated and measured results are in reasonable agreement. In fact, this correlation might also simply be a nice coincidence, because the subdivision into thermal and non-thermal electrons is a bit artificial, at least in the modeling network (cf. Fig. 8, where the EEDF ranges from thermal to maximum energy). Indeed, from the modeling point of view, the fluid model is most suitable for calculating the electron density, whereas the Monte Carlo model is most reliable for providing information on the non-thermal electrons, and in particular on their energy, and their role in inelastic collision processes in the discharge.

The average electron energy, as calculated in the Monte Carlo model, is plotted as a function of distance from the cathode in Fig. 10, for the six different conditions under study. Every figure also contains an inset, which shows in detail the behavior of the average energy in the CDS (note the different  $x$ -scale, in mm). At all conditions, the average electron energy increases rapidly in the CDS, and reaches a maximum at the end of the CDS, where the electrons have gained most

energy from the potential drop. Then, the energy drops again quickly to values on the order of 10–30 eV in the entire NG, as the electrons lose their energy by collisions. The maximum value of the average electron energy, at the end of the CDS, increases with the discharge voltage, and is typically on the order of 60–80% of the discharge voltage. This fraction increases slightly for lower pressures (since less energy is lost by collisions) and for higher voltages (because the average energy is then above the value corresponding to the maximum cross-section, so that collisions also become less frequent). Note that the calculated average electron energy, even in the NG, is much higher than the measured values [4]. However, it is calculated from the entire electron population, including electrons with energy corresponding to the total discharge voltage, and these high-energy electrons could not be observed in the experiment. Hence, it appears that the information about the electron energy and the EEDF, as obtained from model and experiment, is rather complementary. The experiment provides information about the thermal and low-energy electrons, whereas the model is more suitable for higher-energy electrons, which are present at lower density in the discharge (and can therefore not be observed in the experiment), but which play the most important role in the discharge for excitation, ionization, and sustaining the discharge.

#### 4. Conclusion

We have applied our modeling network to the experimental operating conditions of Paper I [4], and we have focused on the gas temperature and resulting current–voltage–pressure relations, as well as on the electron characteristics (density, EEDF and average energy).

The gas-temperature distribution is calculated in the model using the power input from the Monte Carlo models. It was shown that the gas temperature depends almost linearly on the assumed cathode temperature. This illustrates one of the weaknesses of the model, since the cathode temperature is generally not known. Therefore, we have adjusted the cathode temperature to obtain a gas-temperature distribution that yields current–voltage–pressure relations in satisfactory correspondence with experiment. The cathode temperature values obtained in this way are in reasonable agreement with an estimate obtained from the experiments. Moreover, the calculated gas temperature distribution is compared with the values obtained from Rayleigh scattering, and from the reasonable agreement between calculated and experimental data, it can be concluded that the model gives realistic predictions for the electrical current, as a function of voltage, pressure and gas temperature, and hence, that the plasma processes are correctly described in the model.

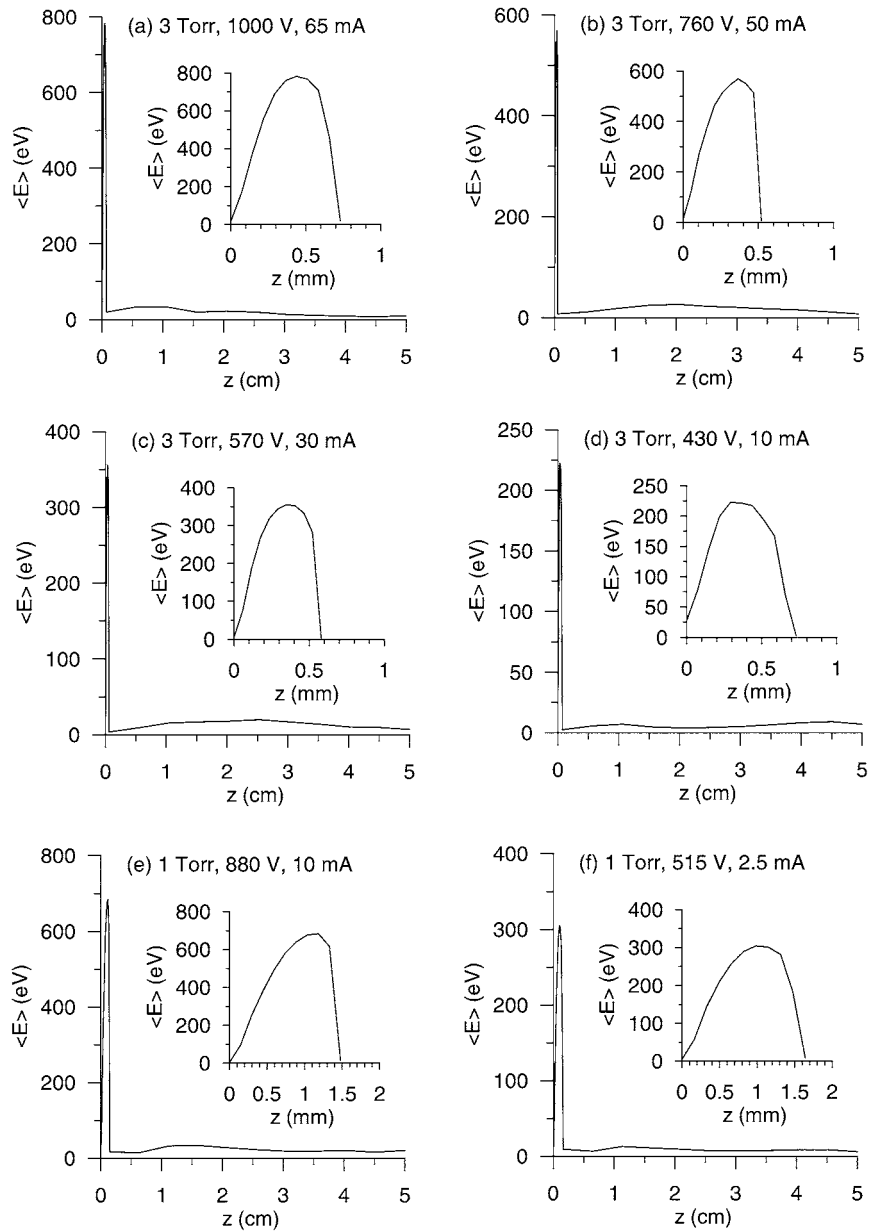


Fig. 10. Calculated average electron energy as a function of distance from the cathode, at six different glow discharge conditions. The insets in the figures show details of the average electron energy in the CDS.

For the electron characteristics, the calculated electron density was found to be in reasonable correlation with the values obtained from the Thomson-scattering experiment. As far as the EEDF and the average electron energy are concerned, comparison between model and experiment cannot be carried out in a simple way. Indeed, the experiment can detect only low-energy electrons, because the high-energy electrons result in signals that are too low. The model, however focuses more on the high-energy electrons, which are most important in the glow discharge plasma, i.e. for excitation, ionization, and sustaining the discharge. Hence, model and experiment can be considered as being

complementary to each other in providing information on the electron energy and EEDF.

In general, the present comparison with experiment has proven to be particularly useful for the model, to verify the calculated results, to give a better idea on the values for input data, as well as to provide complementary information on certain plasma quantities.

### Acknowledgments

A. Bogaerts acknowledges financial support from the Flemish Fund for Scientific Research (FWO), and for supporting her research visit at Indiana University, as

well as from the Belgian Federal Services for Scientific, Technical and Cultural Affairs (DWTC/SSTC) of the prime Minister's Office through the IUAP-V program. Supported in part also by the US Department of Energy through grant DE-FG02-98ER 14890.

## References

- [1] R.K. Marcus, *Glow Discharge Spectroscopies*, Plenum, New York, 1993.
- [2] R. Payling, D.G. Jones, A. Bengtson, *Glow Discharge Optical Emission Spectrometry*, Wiley, Chichester, 1997.
- [3] R.K. Marcus, J.A.C. Broekaert, *Glow Discharge Plasmas in Analytical Spectroscopy*, Wiley, Chichester, 2003.
- [4] G. Gamez, A. Bogaerts, F. Andrade, G.M. Hieftje, Fundamental studies on a planar-cathode direct current glow discharge: Part I: characterization via laser scattering techniques, *Spectrochim. Acta Part B*, 59 (2004) 435–447.
- [5] A. Bogaerts, Comprehensive modelling network for d.c. glow discharges in argon, *Plasma Sources Sci. Technol.* 8 (1999) 210–229.
- [6] A. Bogaerts, R. Gijbels, Modeling of argon direct current glow discharges and comparison with experiment: how good is the agreement?, *J. Anal. At. Spectrom.* 13 (1998) 945–953.
- [7] A. Bogaerts, E. Wagner, B.W. Smith, J.D. Winefordner, D. Pollmann, W.W. Harrison, R. Gijbels, Three-dimensional density profiles of sputtered atoms and ions in a direct current glow discharge: experimental study and comparison with calculations, *Spectrochim. Acta Part B* 52 (1997) 205–218.
- [8] A. Bogaerts, J. Naylor, M. Hatcher, W.J. Jones, R. Mason, Influence of sticking coefficients on the behavior of sputtered atoms in an argon glow discharge: modeling and comparison with experiment, *J. Vac. Sci. Technol. A* 16 (1998) 2400–2410.
- [9] A. Bogaerts, R.D. Guenard, B.W. Smith, J.D. Winefordner, W.W. Harrison, R. Gijbels, Three-dimensional density profiles of argon metastable atoms in a direct current glow discharge: experimental study and comparison with calculations, *Spectrochim. Acta Part B* 52 (1997) 219–229.
- [10] A. Bogaerts, R. Gijbels, Comprehensive description of a Grimm-type glow discharge source used for optical emission spectrometry: a mathematical simulation, *Spectrochim. Acta Part B* 53 (1998) 437–462.
- [11] A. Bogaerts, R. Gijbels, Calculation of crater profiles on a flat cathode in a direct current glow discharge, and comparison with experiment, *Spectrochim. Acta Part B* 52 (1997) 765–778.
- [12] A. Bogaerts, L. Wilken, V. Hoffmann, R. Gijbels, K. Wetzig, Comparison of modeling calculations with experimental results for direct current glow discharge optical emission spectrometry, *Spectrochim. Acta Part B* 56 (2001) 551–564.
- [13] A. Bogaerts, Z. Donko, K. Kutasi, G. Bano, N. Pinhao, M. Pinheiro, Comparison of calculated and measured optical emission intensities in a direct current argon–copper glow discharge, *Spectrochim. Acta Part B* 55 (2000) 1465–1479.
- [14] A. Bogaerts, L. Wilken, V. Hoffmann, R. Gijbels, K. Wetzig, Comparison of modeling calculations with experimental results for r.f. glow discharge optical emission spectrometry, *Spectrochim. Acta Part B* 57 (2002) 109–119.
- [15] A.V. Phelps, Z.L.j. Petrovic, Cold-cathode discharges and breakdown in argon: surface and gas phase production of secondary electrons, *Plasma Sources Sci. Technol.* 8 (1999) R21–R44.
- [16] A. Bogaerts, R. Gijbels, The ion- and atom-induced secondary electron emission yield: numerical study for the effect of clean and dirty cathode surfaces, *Plasma Sources Sci. Technol.* 11 (2002) 27–36.
- [17] M. Surendra, D.B. Graves, G.M. Jellum, Self-consistent model of a direct-current glow discharge: treatment of fast electrons, *Phys. Rev. A* 41 (1990) 1112–1125.
- [18] A. Fiala, L.C. Pitchford, J.P. Boeuf, Two-dimensional hybrid model of low-pressure glow discharges, *Phys. Rev. E* 49 (1994) 5607–5622.
- [19] Z. Donko, Hybrid model of a rectangular hollow cathode discharge, *Phys. Rev. E* 57 (1998) 7126–7137.
- [20] A. Bogaerts, R. Gijbels, W.J. Goedheer, Hybrid Monte Carlo – fluid model of a direct current glow discharge, *J. Appl. Phys.* 78 (1995) 2233–2241.
- [21] A. Bogaerts, R. Gijbels, V.V. Serikov, Calculation of gas heating in direct current argon glow discharges, *J. Appl. Phys.* 87 (2000) 8334–8344.
- [22] A. Bogaerts, M. van Straaten, R. Gijbels, Monte Carlo simulation of an analytical glow discharge: motion of electrons, ions and fast neutrals in the cathode dark space, *Spectrochim. Acta Part B* 50 (1995) 179–196.
- [23] A. Bogaerts, R. Gijbels, The role of fast argon ions and atoms in the ionization of argon in a direct-current glow discharge: a mathematical simulation, *J. Appl. Phys.* 78 (1995) 6427–6431.
- [24] N. Matsunami, Y. Yamamura, Y. Itikawa, N. Itoh, Y. Kazumata, S. Miyagawa, K. Morita, R. Shimizu, H. Tawara, Energy dependence on the ion-induced sputtering yields of monoatomic solids, *At. Data Nucl. Data Tables* 31 (1984) 1–80.
- [25] A. Bogaerts, M. van Straaten, R. Gijbels, Description of the thermalization process of the sputtered atoms in a glow discharge using a three-dimensional Monte Carlo method, *J. Appl. Phys.* 77 (1995) 1868–1874.
- [26] G. Gamez, M. Huang, S.A. Lehn, G.M. Hieftje, Laser-scattering instrument for fundamental studies on a glow discharge, *J. Anal. At. Spectrom.* 18 (2003) 680–684.
- [27] M. Kuraica, N. Konjevic, M. Platasa, D. Pantelic, Plasma diagnostics of the Grimm-type glow discharge, *Spectrochim. Acta Part B* 47 (1992) 1173–1186.
- [28] N.P. Ferreira, H.G.C. Human, L.R.P. Butler, Kinetic temperatures and electron densities in the plasma of a side view Grimm-type glow discharge, *Spectrochim. Acta Part B* 35 (1980) 287–295.
- [29] J.M. Brackett, J.C. Mitchell, T.J. Vickers, Temperature and electron density measurements in a d.c. glow discharge, *Appl. Spectrosc.* 38 (1984) 136–140.
- [30] D. Fang, R.K. Marcus, Use of a cylindrical Langmuir probe for the characterization of charged particle populations in a planar, diode glow discharge device, *Spectrochim. Acta Part B* 45 (1990) 1053–1074.
- [31] D. Fang, R.K. Marcus, Effect of discharge conditions and cathode identity on charged particle populations in the negative glow region of a simple diode glow discharge, *Spectrochim. Acta Part B* 46 (1991) 983–1000.
- [32] A. Bogaerts, A. Quentmeier, N. Jakubowski, R. Gijbels, Plasma diagnostics of an analytical Grimm-type glow discharge in argon and in neon: Langmuir probe and optical emission spectrometry measurements, *Spectrochim. Acta Part B* 50 (1995) 1337–1349.
- [33] A. Bogaerts, R. Gijbels, Comprehensive description of a Grimm-type glow discharge source used for optical emission spectrometry: a mathematical simulation, *Spectrochim. Acta Part B* 53 (1998) 437–462.
- [34] A. Bogaerts, R. Gijbels, W.J. Goedheer, Two-dimensional model of a direct current glow discharge: description of the electrons, argon ions and fast argon atoms, *Anal. Chem.* 68 (1996) 2296–2303.
- [35] P. Gill, C.E. Webb, Electron energy distributions in the negative glow and their relevance to hollow cathode lasers, *J. Phys. D: Appl. Phys.* 10 (1977) 299–311.